Molecular Pharmacology Fast Forward. Published on August 7, 2019 as DOI: 10.1124/mol.119.116806
This article has not been copyedited and formatted. The final version may differ from this version.

First High-Resolution Crystal Structures of the Glucocorticoid Receptor Ligand-Binding Domain–PGC1α Complex with Endogenous and Synthetic Glucocorticoids

Xu Liu, Yashuo Wang and Eric A. Ortlund

Department of Biochemistry, Emory University School of Medicine, Atlanta GA 30322 USA (X.L., Y.W., E.A.O.); College of Life Sciences, Qingdao University, Qingdao 266071, China (Y.W.)

Molecular Pharmacology Fast Forward. Published on August 7, 2019 as DOI: 10.1124/mol.119.116806
This article has not been copyedited and formatted. The final version may differ from this version.

Running title: Structural analyses of GR LBD-ligand-PGC1α complexes.

*Correspondence:

Eric A. Ortlund, Department of Biochemistry, Emory University School of Medicine, 1510 Clifton Road NE, Rollins Research Center G235, Atlanta, GA 30322

E-mail: eortlun@emory.edu

Phone: 404-727-5014

Fax: 404-727-2738

Abbreviations: Dexamethasone, DEX; Glucocorticoid Receptor, GR; Hydrocortisone, HCY; hydrogen-deuterium exchange, HDX; ligand binding domain, LBD; nuclear co-repressor, NCoR; Nuclear Receptor, NR; Nuclear Receptor Coactivator-2, Tif2; peroxisome proliferator-activated gamma coactivator 1-α, PGC1α; Protein Data Bank, PDB; Root Mean Square Fluctuation, RMSF; silencing mediator of retinoic acid and thyroid hormone receptor, SMRT.

Abstract

Both synthetic and endogenous glucocorticoids are important pharmaceutical drugs known to bind to the ligand binding domain (LBD) of glucocorticoid receptor (GR), a member of the nuclear receptor (NR) superfamily. Ligand binding induces conformational changes within GR, resulting in subsequent DNA binding and differential co-regulator recruitment, ultimately activating or repressing target gene expression. One of the most crucial co-regulators is peroxisome proliferator-activated gamma coactivator 1-α (PGC1α), which acts to regulate energy metabolism by directly interacting with GR to modulate gene expression. However, the mechanisms through which PGC1α senses GR conformation to drive transcription are not completely known. Here, an ancestral variant of the GR (AncGR2) LBD was utilized as a tool to produce stable protein for biochemical and structural studies. PGC1α is found to interact more tightly and form a more stable complex with AncGR2 LBD than Tif2. We report the first high resolution X-ray crystal structures of AncGR2 LBD in complex with PGC1α and dexamethasone or hydrocortisone. Structural analyses reveal how distinct steroid drugs bind to GR with different affinities by unique hydrogen bonds and hydrophobic interactions. Important charge clamps are formed between the activation function-2 (AF-2) and PGC1α to mediate their specific interactions. These interactions lead to a high level of protection from hydrogen-deuterium exchange at the coregulator interaction site and strong intramolecular allosteric communication to ligand binding site. This is the first structure detailing the GR- PGC1α interaction providing a foundation for future design of specific therapeutic agents targeting these critical metabolic regulators.

Significance Statements

High resolution structures of AncGR2 LBD bound to DEX and HCY in complex with PGC1α are determined, which reveal the molecular mechanism of PGC1α binding to AncGR2 LBD as well as the distinct affinities between DEX and HCY binding. Identifying the structural mechanisms that drive drug affinity is of pharmacological interest to the glucocorticoid receptor field as an avenue to guide future drug design targeting GR-PGC1α signaling that plays crucial roles in controlling hepatic glucose output.

Molecular Pharmacology Fast Forward. Published on August 7, 2019 as DOI: 10.1124/mol.119.116806
This article has not been copyedited and formatted. The final version may differ from this version.

Introduction

Glucocorticoid receptor (GR) is a ligand-regulated transcription factor that plays key roles in inflammation, metabolism, and immunity (Kadmiel and Cidlowski, 2013). GR consists of a N-terminal domain (NTD), a DNA binding domain (DBD), a flexible hinge region, and a C-terminal ligand binding domain (LBD) (Hollenberg et al., 1985). The highly disordered NTD is required for full transcriptional activity through ligand-independent interaction with coregulators (Hollenberg and Evans, 1988). GR DBD recognizes both positive and negative glucocorticoid response elements (GREs) to facilitate target gene activation or repression (Weikum et al., 2017a). GR ligands bind to the ligand binding pocket (LBP) within the LBD and allosterically stablize the distal activation function-2 (AF-2) region comprised of helices 3, 4 and 12. The AF-2 region can interact with different coactivators that contain a conserved LXXLL motif or corepressors that present a conserved LXXX(I/L)XXX(I/L) motif (L- leucine, I-isoleucine, X-any amino acid). Helix 12 in the AF-2 region is termed the activation function helix (AF-H) and can switch between different conformations to favor differential binding to coactivators and corepressors (Kauppi et al., 2003; Schoch et al., 2010).

In response to stress or low blood sugar, the adrenal gland secretes cortisol (also known as hydrocortisone: HCY), a cholesterol-derived glucocorticoid that functions to induce glucose uptake, regulate metabolism and suppress the immune system (Chrousos, 2009) (**Figure 1A**). HCY is clinically used as an anti-inflammatory agent, but this endogenous hormone is rapidly metabolized and drives off-target gene activation via the closely related mineralocorticoid receptor in some tissue. Synthetic glucocorticoids, including triamcinolone acetonide (TA), mometasone furoate (MOF), and dexamethasone (DEX), typically have improved therapeutic effects for inflammatory and autoimmune disease compared to HCY. However, both HCY and

Molecular Pharmacology Fast Forward. Published on August 7, 2019 as DOI: 10.1124/mol.119.116806
This article has not been copyedited and formatted. The final version may differ from this version.

synthetic glucocorticoids can have adverse side effects when they're used in high dose and prolonged period, such as weight gain, Cushing's syndrome, and osteoporosis. GR-mediated transactivation is believed to be the predominant molecular mechanism involved in side effects (Schacke et al., 2002). Design of new dissociated GR ligands that preferentially induce transrepression rather than transactivation to achieve significant clinical benefits with reduced side effects are expected to be the future of corticoid-driven treatment (Schacke et al., 2005).

Peroxisome proliferator-activated gamma coactivator 1-α (PGC1α) was first identified as a coactivator for peroxisome proliferator-activated receptor γ (PPARγ) (Puigserver et al., 1998). Since then, PGC1α has been demonstrated to play crucial roles in regulating glucose, lipid, energy metabolism, adaptive thermogenesis, and mitochondrial biogenesis (Bostrom et al., 2012; Knutti and Kralli, 2001; Lin et al., 2005). Human PGC1α was first found to enhance transcription when treated with a GR agonist. The GR LBD interacts with PGC1α's N-terminal domain containing a NR interaction motif. Together, these data suggest PGC1α acts as a coactivator for GR (Knutti et al., 2000). A subsequent study found that the expression of PGC1α was strongly induced in the livers of fasting mice or in primary hepatocytes with DEX treatment , indicating its role in controlling hepatic glucose output. Indeed, PGC1α can coactivate both GR and hepatic nuclear factor-4α to increase transcriptional activation of phosphoenolpyruvate carboxykinase, the rate-limiting enzyme in gluconeogenesis (Yoon et al., 2001).

There are only three structural investigations of PGC1α binding to LBDs from two NRs - liver receptor homolog-1 (LRH-1) and PPARγ (Li et al., 2008; Mays et al., 2017; Yamamoto et al., 2018). How PGC1α interacts with the GR LBD is still unknown. Soluble expression of hGR from *Escherichia coli* (*E.coli*) is challenging and many mutations must be introduced to promote folding and crystallization (He et al., 2014; Schoch et al., 2010). These mutations, identified via

random mutagenesis, may not faithfully capture the allostery driven by ligand binding to the wtGR (Seitz et al., 2010). Here we use the reconstructed ancestral GR protein (AncGR2) which represents the ~420 million year old common ancestor of all bony vertebrates including ray- and lobe-finned fish. The sequence of AncGR2 LBD was constructed by maximum likelihood phylogenetics and shares 80% identity and 96% similarity with hGR, with all residues in the LBP conserved (Bridgham et al., 2009) (**Supplemental Figure 1**). AncGR2 has been used successfully in prior studies to understand the structural basis of ligands and coregulator binding (Bridgham et al., 2009; Kohn et al., 2012; Weikum et al., 2017b). We present the first high resolution structures of AncGR2 LBD with DEX and HCY in complex with PGC1α. Unique charge clamps were identified that may contribute to the recognition of PGC1α by GR, leading to the formation of a more stable complex with strong allosteric communications between ligand and coactivator binding sites.

Materials and Methods

Protein Expression and Purification

Maltose-binding protein (MBP)-fused ancestrally reconstructed GR LBD (GR2 LBD) with a decahistidine tag was expressed and purified as previously reported with some modifications (Weikum et al., 2017b). Briefly, protein was expressed in *E. coli* BL21(pLysS) cells by adding 0.3 mM isopropyl-1-thio-D-galactopyranoside (IPTG) and 50 μM DEX or HCY for induction at 16 °C overnight. After cells lysis by sonication on ice, his-tagged fusion protein was purified by His-Trap affinity chromatography. For ligand binding assays, MBP fused-GR2 LBD was purified by Superdex 200 (S200) size exclusion chromatography (GE Healthcare) in a buffer containing 20 mM HEPES pH 7.4, 150 mM NaCl, 1 mM EDTA, 5 mM DTT, and 0.005 % Tween-20. For all other assays, the MBP-his tag was removed by recombinant Tobbaco Etch

Molecular Pharmacology Fast Forward. Published on August 7, 2019 as DOI: 10.1124/mol.119.116806
This article has not been copyedited and formatted. The final version may differ from this version.

Virus (rTEV) protease cleavage. Undigested fusion protein, cleaved tag, and His-tagged rTEV were separated from the digested AncGR2 LBD by His-Trap affinity chromatography. AncGR2 LBD was further purified by Superdex 75 (S75) size exclusion chromatography (GE Healthcare). Protein was concentrated to 3-5 mg/mL, snap-frozen in liquid nitrogen and stored at -80 °C for later use.

Protein Crystallization, Data Collection and Structure Determination

GR2 LBD in 20 mM HEPES (pH 7.4), 200 mM NaCl and 5 % glycerol was concentrated to 4 mg/mL. Crystallization trials were performed by the hanging-drop vapor diffusion method at 16 °C using 1 µL of precipitant and 1 µL of protein in the presence of two molar equivalents of PGC1α NR Box 2 peptide (NH_2-EEPSLLKKLLLAPA-COO^-). Crystals of the AncGR2 LBD-Dex were formed in 0.3 M sodium chloride, 2.6 M sodium formate and 0.1 M PIPES pH 7.0, whereas AncGR2 LBD-HCY crystals were obtained in 0.05 M sodium thiocyanate, 0.95 M sodium tartrate dibasic dehydrate and 0.1M HEPES pH 7.5. Prior to data collection, crystals were soaked for 5 s in mother liquor containing 25% glycerol and flash-frozen in liquid nitrogen. Diffraction data were collected remotely from the South East Regional Collaborative Access Team (SER-CAT) ID-22 beamline at the Advanced Photon Source (APS) at Argonne National Laboratories at 100 K.

Indexing, integration, and scaling were performed using HKL-2000 (Otwinowski and Minor, 1997). The program Phaser-MR (Adams et al., 2010) was used for molecular replacement using the structure of GR2-Dex-Tif2-peptide complex (Protein Data Bank [PDB code 3GN8) as an initial search model (Bridgham et al., 2009). Structure refinement and model building were performed using PHENIX (v1.12) and COOT (Emsley and Cowtan, 2004). PyMOL (v1.8.2) was used to visualize structures, perform alignments and generate figures (Schrödinger, LLC).

Molecular Pharmacology Fast Forward. Published on August 7, 2019 as DOI: 10.1124/mol.119.116806
This article has not been copyedited and formatted. The final version may differ from this version.

Hydrogen bonds and hydrophobic contacts were identified by Ligplot (v.4.5.3) (Wallace et al., 1995). Conformational structural analysis was performed using ProSMART (v.0.845) (Nicholls et al., 2014).

Differential Scanning Fluorimetry (DSF)

DSF was performed using a StepOne Plus Real Time PCR System (ThermoFisher). AncGR2 LBD in 20 mM Tris (pH 7.4), 300 mM NaCl, and 5 % glycerol at 10 μM was used. Protein was incubated with 50 μM DEX or HCY, 50 μM co-regulator peptides and SYPRO® orange dye (Sigma) at a final 1:1000 dilution. The peptide sequences used were as follows: Tif2 NR Box 3 (NH2-KENALLRYLLDKDD-COO^-), SMRT (NH2-TNMGLEAIIRKALMGKY-COO^-) and NCoR ID2 (NH2-DPASNLGLEDIIRKALMGSFDDK-COO^-). Temperature scans were performed from 25 °C to 95 °C at a rate of 0.5 °C/min and fluorescence was monitored using the ROX filter (602 nm). Three technical replicates and three biological replicates were conducted. The data were normalized and fit to a two-state model with a single transition between native and denatured protein using Boltzmann sigmoidal curve as previously described (Weikum et al., 2017b).

Fluorescence Polarization Binding Assays

N-terminal FAM-labelled coregulator peptides, with sequences shown above, were used at a final concentration of 50 nM in the assay buffer containing 20mM HEPES (pH 7.4), 150 mM NaCl and 5 % glycerol. Increasing concentration of GR2LBD was added into labelled peptides with fluorescence polarization signal monitored using a BioTek Neo plate-reader (Winooski, VT) at an excitation and emission wavelength of 485 and 528 nm, respectively. Three technical replicates and three biological replicates (i.e. three separate preparations of protein) were conducted and graphs are a compilation of all data collected. Binding data were fit

Molecular Pharmacology Fast Forward. Published on August 7, 2019 as DOI: 10.1124/mol.119.116806
This article has not been copyedited and formatted. The final version may differ from this version.

with a one-site specific binding curve [$Y=B_{max}*X/(K_d+X)$] in GraphPad Prism v8 (GraphPad, Inc).

Competition binding assays were performed using 100 nM MBP-fused GR2LBD in the presence of 12 nM FAM-labelled DEX. Increasing amounts of unlabeled DEX and HCY ligands were added into solution with fluorescence polarization signal recorded as mentioned above. Three technical replicates and three biological replicates using three separate preparations of proteins were conducted and graphs are a compilation of all data collected. Binding data were fit with one-site Ki-fit curve in GraphPad Prism v8 (GraphPad, Inc).

Hydrogen-Deuterium Exchange-Mass Spectrometry (HDX-MS)

HDX-MS was performed using a UPLC HDX system coupled with a Q-Tof Premier mass spectrometer and a robotic autosampler (Waters Corp, Milford, MA) as previously described (Deng et al., 2017). Exchange reaction was initialized by diluting each protein sample (at 2 mg/ml) 1:7 (v/v) into 10 mM phosphate buffer in 99.9 % D_2O. After 0, 10, 100, 1000 and 10000 seconds, equal volume of quenching buffer [100 mM phosphate, 0.5 M tris(2-carboxyethyl) phosphine, 0.8% formic acid, and 2% acetonitrile, pH 2.5] precooled at 1 °C was added to stop the exchange reaction. Reactions at each time point were performed in triplicate. Quenched samples were fragmented by passing through an Enzymate BEH pepsin column (Waters Corp, Milford, MA) and further separated by an in-line C18 UPLC column and analyzed by MS. Peptides were identified through database searching of AncGR2 LBD sequence using ProteinLynx Global SERVER™ (PLGS). The HDX-MS data were processed in DynamX (v3.0) and the HDX difference between different states was calculated by comparing the relative fractional uptake for each residue at a given time.

Molecular Dynamics Simulations

Molecular Pharmacology Fast Forward. Published on August 7, 2019 as DOI: 10.1124/mol.119.116806
This article has not been copyedited and formatted. The final version may differ from this version.

Molecular dynamics simulations were conducted as previously described (Mays et al., 2017). Briefly, GR2-HCY, GR2-DEX, GR2-DEX-Tif2 and GR2-DEX-PGC1α complexes were solvated in an octahedral box of TIP3P water with 10 Å buffer surrounding it. Na^+ and Cl^- ions were added to a final concentration of 150 mM to neutralize the protein. All minimizations and 1000 ns simulations were performed with Amber18 (D.A. Case, 2018) using a 2 fs timestep. All bonds between heavy atoms and hydrogens were fixed with the SHAKE algorithm (Ryckaert et al., 1977). Twenty-five thousand evenly spaced frames were taken from each simulation for further analysis. Root mean square fluctuations (RMSF) were calculated on Cα atoms of protein residues for each frame in the trajectory using the initial structure as the reference. Ligand C_2 atom and all protein Cα atoms in a system were defined as nodes for dynamical networks analysis. Edges are drawn between a pair of nodes when they are within 4.5 Å for at least 75 % of MD simulation trajectory. Cartesian covariance and correlation between two nodes were calculated using Carma program (Glykos, 2006). The edge distances were derived from pairwise correlations as a measure of communication within the network. Suboptimal paths between ligand and AFH regions were identified using the Floyd-Warshall algorithm (Floyd, 1962) and subopt program in NetworkView plugin in VMD (Humphrey et al., 1996).

Reporter Gene Assays

HeLa cells were maintained and passaged in α-minimal essential medium (Life Technologies) supplemented with 10 % stripped FBS (Invitrogen). Cells grown in 96-well plates were transfected at 70 % confluence with 10 ng of GR, 50 ng of 6X GRE firefly luciferase reporter, and 1 ng of Renilla luciferase reporter under the control of the constitutively active pRL-CMV promoter. For transfection, OptiMEM media was used with FuGeneHD (Roche Applied Science). Twenty-four hours after transfection, cells were treated with different

Molecular Pharmacology Fast Forward. Published on August 7, 2019 as DOI: 10.1124/mol.119.116806
This article has not been copyedited and formatted. The final version may differ from this version.

concentrations of drugs or vehicle (DMSO) in triplicate. Renilla and firefly luciferase activities were measured 24 hours after drug treatment using the DualGlo kit (Promega) by a BioTek Neo plate-reader (Winooski, VT). Transactivation data were fit with log(agonist) *vs* response curve in GraphPad Prism v8 (GraphPad, Inc).

Results

Higher Affinity for DEX vs HCY is Preserved in AncGR2

DEX resembles the classical glucocorticoid structure of HCY differing in three key ways: the A ring contains a C-C double bond between C_1 and C_2; a fluorine atom is located at C_9 in the B ring and the D ring contains a methyl group ($-CH_3$) at C_{16} (**Figure 1A and B**). These structural differences enable two-fold tighter binding of DEX to the AncGR2 LBD vs HCY (K_i = 20 nM [95% confidence interval: 17, 26] (20 nM [17,26]) *vs* 43 nM [36,52]) (**Figure 1C**) as measured in a FP-based competitive binding assay. DEX is ~10-fold more potent than HCY in gene transactivation from a GRE (HCY EC_{50} 1.3 nM *vs* Dex EC_{50} 15 nM), which is consistent with previous reports report (He et al., 2014) (**Figure 1D**). This is consistent with clinical usage of DEX as a more potent, efficacious and long-acting drug compared to HCY (Zoorob and Cender, 1998).

High Resolution Crystal Structures of AncGR2 LBD with Ligands and PGC1α

Crystallization of human GR is challenging and requires the use GR mutants with enhanced solubility and crystallization properties. We leveraged the ancestrally reconstructed AncGR2 which behaves faithfully in its ligand binding, response and allostery but shows enhanced expression, solubility and crystallization (Bridgham et al., 2009; Kohn et al., 2012; Weikum et al., 2017b). To understand the molecular determinants of PGC1α binding to GR, we determined the X-ray crystal structures of AncGR2 LBD with PGC1α in complex with both

Molecular Pharmacology Fast Forward. Published on August 7, 2019 as DOI: 10.1124/mol.119.116806
This article has not been copyedited and formatted. The final version may differ from this version.

DEX and HCY ligands. Both crystals formed in the $C222_1$ space group with one AncGR2 LBD molecule in the asymmetric unit. The structure of AncGR2 LBD-DEX-PGC1α trimeric complex was refined to 1.64 Å (**PDB File 1**) and that of AncGR2 LBD-HCY-PGC1α complex was refined to 1.60 Å (**PDB File 2**) (**Table 1**). This represents the highest resolution GR LBD-ligand complexes to date, indicating the benefit of using an ancestrally reconstructed sequence variant for crystallography studies (Bledsoe et al., 2002; Bridgham et al., 2009; He et al., 2014; Kohn et al., 2012; Suino-Powell et al., 2008; Weikum et al., 2017b).

Overall, AncGR2 LBD adopts the classical NR/SR structure, consisting of a helical sandwich with three layers, including 11 α helices and four β strands (**Figure 2A**). The PGC1α coactivator peptide forms a short α helix and binds to the AF-2 region formed by helix 3, helix 4, and helix 12 (AF-H). Both DEX and HCY ligands occupy in the LBP at the base of AncGR2 LBD, as supported by unambiguous electron density (**Figure 2B and C**). The glucocorticoid ligands make extensive hydrophobic interactions and the carbonyl O_1 on the A ring of the ligand participates in a hydrogen bond network with Gln39 and Arg80 and a structurally conserved water molecule (**Supplemental Figure 2A)**. Residue Gln111 makes hydrogen bond with hydroxyl O_3 on the D ring. Residue Asn33 hydrogen bonds with both hydroxyls O_2 and O_5. Likewise, residue Thr208 makes two hydrogen bonds with atoms O_4 and O_5 on the D ring (**Figure 2D and E**).

The AncGR2 LBD HCY-PGC1α and AncGR2 LBD DEX-PGC1α complexes show very little conformational variation. The root mean square deviation (RMSD) between these structures is 0.12 Å out of 212 Cα atoms. The residues in the N-terminal loop, the loops preceding helix 3, between helix 9 and 10, together with the short helix 6 and its surrounding loops are the only regions with high RMSDs **(Supplemental Figure 3A**). ProSMART analysis, which compares

Molecular Pharmacology Fast Forward. Published on August 7, 2019 as DOI: 10.1124/mol.119.116806
This article has not been copyedited and formatted. The final version may differ from this version.

local structural similarity over a sliding window of 7-9 residues, confirmed high similarity in most structural elements with differences in the areas omitted from the RMSD analysis (**Supplemental Figure 3B)** (Nicholls et al., 2014).

Detailed structure comparison between the DEX- and HCY-bound AncGR2 LBD complexes provides insight into molecular determinants of their observed differences in binding affinity and transactivation efficacy. The double bond between C_1 and C_2 in DEX results in a stronger interaction between the ligands O_1 atom and Gln39 (hydrogen bond distance as 3.0 Å in DEX *vs* 3.4 Å in HCY) (**Figure 2D and E**). The fluorine atom at C_9 of the B ring in DEX makes closer contact to residues Leu32, Phe92, and Met115 than the hydrogen atom in same position in HCY (**Supplemental Figure 2B and C**). Likewise, the additional CH_3 group at C_{16} in DEX makes closer contact to residues Leu201, Phe204, Glu111, and Met115 than the hydrogen atom in same position in HCY (**Supplemental Figure 2D and E**). In contrast to DEX, HCY makes no hydrophobic contacts with aliphatic residues Met115 and Leu201 (**Figure 2D and E**). Taken together, HCY makes weaker hydrogen bonds and fewer hydrophobic contacts *vs* DEX explaining the weaker affinity for the AncGR2 LBD.

PGC1α Binds the holo-GR2 LBD with affinity similar to Tif2

We determined the binding affinities for various FAM-labelled coregulator peptides on AncGR2 LBD – DEX/HCY complexes (**Figure 3**). AncGR2 LBD bound slightly better to PGC1α than to Tif2 in complex with either ligand (K_d = 0.31 *vs* 0.57 μM in presence of DEX; K_d = 0.52 *vs* 0.97 μM in presence of HCY) (**Figure 3 A and C**). In line with in cell and *in vivo* data, HCY induced weaker association with all coregulators tested relative to DEX (**Figure 3B and D**). As expected, AncGR2 LBD – agonist complexes bound to coactivators more tightly than to corepressors (**Figure 3**).

Molecular Pharmacology Fast Forward. Published on August 7, 2019 as DOI: 10.1124/mol.119.116806
This article has not been copyedited and formatted. The final version may differ from this version.

PGC1α Stabilizes AncGR2 LBD More Than Other Coregulators

Glucocorticoid ligands are known to increase the stability of the GR LBD and therefore are used in its expression and purification (Bledsoe et al., 2002). Here we used differential scanning fluorimetry (DSF)-based thermal denaturation to determine the melting temperature (T_m) as a reporter of protein complex stability. We examined AncGR2 LBD's thermostability in the presence of different ligands and coregulators. The AncGR2 LBD-DEX complex is more stable than the AncGR2 LBD-HCY complex (Tm=54.5 °C *vs* 52.5 °C, respectively) **(Figure 4A and C**). When the AncGR2 LBD is bound to DEX or HCY, both Tif2 and PGC1α increased the protein stability, whereas NCoR and SMRT had no effect (**Figure 4B and D**). Upon coactivator binding, PGC1α stabilizes the complex by 2.5 and 3.3 °C more than Tif2 in the DEX- and HCY-bound AncGR2 LBD (Tm=58.5 °C *vs* 56.0 °C; Tm=57.5 °C *vs* 54.2 °C), respectively (**Figure 4**).

GR2 Recognizes PGC1α by Unique Hydrophobic Contacts and a Secondary Charge Clamp

Both PGC1α box2 (NH_2-$_{141}$PSLLKKLLLAPA$_{152}$-COO^-) and Tif2 box3 peptides (NH_2-$_{742}$NALLRYLLDKD$_{752}$-COO^-) contain a consensus LXXLL motif and bind to the AncGR2 LBD at the AF-2 site. Residues Val44, Lys45, Leu58, Met62, Gln66, Glu220 and Met221 from AncGR2 LBD form a hydrophobic groove and make hydrophobic interactions with Leu143, Leu144, Leu147, Leu148, Leu149 and Ala152 from PGC1α (**Figure 5A**). Comparison of the previously determined AncGR2 LBD-Tif2 structure (PDB 3GN8) shows that all residues except for Leu58 from helix4 are involved in Tif2 recognition groove. Tif2 fails to interact with Leu58 as it contains an Asp750 at the equivalent position of PGC1α Leu149, which would result in a polar incompatibility (**Figure 5B**).

To hold coactivators in position, SR LBDs form hydrogen bonds with the C- and N-termini of the NR box-containing peptides. These conserved interactions are described as

Molecular Pharmacology Fast Forward. Published on August 7, 2019 as DOI: 10.1124/mol.119.116806
This article has not been copyedited and formatted. The final version may differ from this version.

primary charge clamps and are crucial for coregulator recognition. For PGC1α, Glu222 from AF-H forms a hydrogen bond with the amide nitrogen from Leu143. Lys48 from helix 3 recognizes the C-terminus of PGC1α by forming hydrogen bonds with backbone carbonyls from Leu147 and Ala150, respectively (**Figure 5C**). However, AncGR2 Lys48 in the Tif2 complex structure moves marginally away from its orientation in the PGC1α complex structure and thus only forms one hydrogen bond with Ala50 (**Figure 5D**). There is a water-mediated hydrogen bond formed between AncGR2 Gln61 and PGC1α Leu148. This is not observed in the AncGR2 LBD Tif2 complex structure (**Figure 5D**). The ability of bound coregulators to form a secondary charge clamp has been observed previously for GR, and it appears that PGC1α leverages this mechanism (Bledsoe et al., 2002). As such, an electrostatic interaction is formed between Asp59 in AncGR2 LBD helix 4 and Lys145 in PGC1α. In Tif2, the side chain of Arg746, which is at a position equivalent to PGC1α Lys145, extends away from AncGR2 Asp59 without forming strong favorable electrostatic interaction (**Figure 5D**). Thus, both additional hydrophobic and charge-charge interactions are involved in the AncGR2 LBD PGC1α interaction likely explaining its ability to stabilize AncGR2 to a greater extent than Tif2 (**Figure 3 and 4**).

PGC1α Binding Rigidifies Local Dynamics around AF-2 Site of AncGR2 LBD

Protein dynamics are crucial for enzyme catalysis, ligand recognition, protein allostery, and molecular evolution (Henzler-Wildman and Kern, 2007; Liu et al., 2016; Motlagh et al., 2014; Tokuriki and Tawfik, 2009). Solution-based studies, including nuclear magnetic resonance (NMR) spectroscopy and hydrogen-deuterium exchange coupled with mass spectrometry (HDX-MS), allow for measuring protein motions to probe conformational fluctuations that are not readily observed in static crystal structures. NR LBDs in their apo states are known to be dynamic. The equilibrium between subtly different conformational states can be shifted by

Molecular Pharmacology Fast Forward. Published on August 7, 2019 as DOI: 10.1124/mol.119.116806
This article has not been copyedited and formatted. The final version may differ from this version.

binding to different ligands and coregualtors, which are believed to play important roles in the mechanism of action of NR ligands (Hughes et al., 2012; Kojetin and Burris, 2013).

Here, we employed HDX-MS to investigate the dynamics of AncGR2 LBD with DEX bound to Tif2 and PGC1α. Overall, 108 peptic fragments from AncGR2 LBD were sequenced and mapped for HDX analysis. These peptides covered 96 % of the AncGR2 LBD sequence with more than 5-fold redundancy (**Supplemental Figure 4)**. Residues at both N- and C-terminal regions, residues 140 and 156 are not covered by any peptides (**Figure 6A**). We found a high percentage of deuterium uptake in AncGR2 LBD (~70%), given the 1:7 dilution of H_2O-containing solution into D_2O. Comparison between Tif2- and PGC1α-bound complexes showed decreased deuterium uptake in the PGC1α-bound state. For instance, residues 58-65, 197-203, and 225-233 showed less deuterium uptake in the PGC1α-bound complex than the Tif2-bound complex (**Figure 6B**). Mapping these residues onto the structure shows that they are in AF-H, helix 4, and helix 10, all of which are in or adjacent to the AF-2 site (**Figure 6C**). This suggests that PGC1α binding produces a higher level of protection from deuterium exchange and thus more pronounced rigidification of the dynamic motions in these regions. Interestingly, some residues in helices 8 and 9, as well as the β4 strand are more flexible in the PGC1α-bound state than the Tif2-bound state. However, these differences are subtle compared those in the AF-2 site. Overall, the PGC1α-bound complex shows more dampened local dynamics, primarily at the AF-2 site, than Tif2-bound complex, which is in accordance with the higher global thermostability of the PGC1α-bound complex (**Figure 4**).

Allosteric Communication between Steroid Ligand and AF-H

Molecular dynamics (MD) simulations were performed to analyze conformational dynamics and allostery within the AncGR2 LBD complexes. During the entire 1 μs simulation,

Molecular Pharmacology Fast Forward. Published on August 7, 2019 as DOI: 10.1124/mol.119.116806
This article has not been copyedited and formatted. The final version may differ from this version.

all AncGR2 LBD molecules were characterized by stable RMSDs of less than 2 Å (**Supplemental Figure 5A and B**). Root mean square fluctuations (RMSFs) were calculated on Cα atoms to measure the protein flexibility. Unsurprisingly, residues at both the N- and C-termini show the largest RMSFs. Moreover, loops before helix 3, between helix 9 and 10 and regions around the short helix 6 display larger RMSFs than the rest of the protein (**Figure 7A and B**). This is consistent with RMSD and ProSMART analyses mentioned above.

We combined dynamical network analysis with the MD simulations to compare the strength of allosteric communication between the ligand and AFH. To construct the network, all protein Cα atoms and the ligand C_2 atom were defined as nodes and a pair of nodes were connected by edges if they have satisfied a given distance requirement (<4.5 Å) for at least 75% of the simulation time (**Figure 7C**). Edge distance is derived from and inversely proportional to the pairwise correlations between two nodes across the simulation trajectory. Therefore, short distances represent strongly correlated nodes, whereas long distances indicate weak correlations between two nodes (Bowerman and Wereszczynski, 2016). Here, we selected the bound ligand and residue Ser227, located in the middle of AF-H, as two nodes to study GR allosteric communication (**Figure 7C**). We identified the optimal (shortest) paths and the top 1000 suboptimal (longer) paths connecting these nodes. These analyses reveal that AncGR2 LBD-HCY has longer path lengths than AncGR2 LBD-DEX, and thus weaker allosteric communication (**Figure 7D and E**). Both Tif2 and PGC1α binding to the AF-2 region result in shorter suboptimal path lengths; however, PGC1α causes shorter suboptimal path lengths, indicating that its binding strengthens communication between ligand and AF-H more than Tif2 (**Figure 7D and F**). Residues in LBP, AF-H and identified allosteric paths connecting these sites, such as Gly36, Asn33, Ile225, Pro219, Leu222, and Gln228, are highly conserved between

hGR and AncGR2 LBDs (**Figure 7C and Supplemental Figure 1**). Thus, the allosteric communication patterns observed here should be conserved in hGRLBD.

Discussion

Cortisol was identified as the endogenous glucocorticoid hormone nearly a century ago (Kendall, 1951). Since then, it has been clinically used to decrease immune response and inflammation. Later, the FDA approved DEX, a more potent synthetic glucocorticoid used for the treatment of asthma, rheumatoid arthritis, and other inflammatory conditions and allergic states. Both drugs target the GR LBD and drive and agonist response. Here, we set out to comprehensively compare HCY and DEX using the ancestral AncGR2 LBD. We confirmed that DEX is more potent *in vitro* with a two-fold lower K_i value than HCY when binding to AncGR2 LBD. A previous study using a ^{3}H radioactive labelling-based competition assay found an almost 10-fold difference in K_i values for the human receptor (He et al., 2014). The assays were performed differently: we used fluorescence-based techniques and purified AncGR2 LBD, whereas He et al used GR-containing cell cytosol; this likely explains the differential observations in binding constants. We show that HCY has approximately 10-fold less potency than DEX in a luciferase-based reporter assay, which is consistent with previous findings for the human receptor (He et al., 2014). Along with this difference in affinity and potency, the AncGR2 LBD - HCY complex is less stable than it with DEX. When DEX is bound, AncGR2 LBD can recruit coactivators, such as Tif2 and PGC1α, with tighter binding affinities versus HCY. MD simulations and dynamic network analysis found stronger communication between the LBP and AF-H when DEX in bound, which is the potential underlying mechanism for better coactivator binding.

Molecular Pharmacology Fast Forward. Published on August 7, 2019 as DOI: 10.1124/mol.119.116806
This article has not been copyedited and formatted. The final version may differ from this version.

Structural comparison between these two agonists in complex with AncGR2 LBD reveals different interactions stemming from differences in their chemical structure and how these interactions are preserved in AncGR2 and extant GR LBDs. The fluorine and methyl moieties in DEX exable more extensive and closer contacts to the receptor versus HCY. A previous structural study at 2.5 Å resolution found that both Arg and Gln residues in the LBP made hydrogen bonds with carbonyl O_1 from HCY. A specific additional water molecule, which was not observed in the DEX complex structure, was required to hold HCY A-ring in position (He et al., 2014). However, this water molecule and water-mediated hydrogen bond network are found in both HCY and DEX complex structures presented here. Moreover, this water is also found to form hydrogen bonds with carbonyl O_1 in the structures of AncGR2 LBD – TA and –MOF complexes (Kohn et al., 2012; Weikum et al., 2017b). Together, these data indicate a general mechanism of having a water molecule in the Arg80 and Gln39-mediated hydrogen bond network to orient the A-ring and recognize O_1, which is not unique to the HCY binding. In our ~1.6 Å resolution structures, we found the A-ring in HCY is extended further away from Gln39 and causes a weaker hydrogen bond relative to DEX which contains an A-ring double bond. This tighter hydrogen bond works in concert with increased hydrophobic contacts enabled by the C9 fluorine atom and the C16 methyl group in DEX likely contributes the most to its enhanced binding affinity. Importantly, using the AncGR2 LBD helps to generate higher-resolution structures than hGR LBD (1.6 Å *vs* 2.5 Å), which in turn provides better understanding of the structural mechanism of glucocorticoid ligand binding and thus better support for rational drug design in the future.

PGC1α plays pivotal roles in controlling mitochondrial biogenesis, glucose uptake, fatty acid oxidation, and metabolism of reactive oxygen species (Handschin and Spiegelman, 2006;

Lin et al., 2002; Scarpulla et al., 2012). It acts through coactivating many nuclear receptors including PPARγ, GR, thyroid hormone receptor (TR), and the farnesoid X receptor (FXR) (Lin et al., 2005; Shin et al., 2003; Zhang et al., 2004). PGC1α has long been known as a GR-coacivator (Knutti et al., 2000); however, the structural basis for the PGC1α - GR LBD had not to be explored. Our structural investigation found several unique interactions formed between AncGR2 LBD and PGC1α, including the electrostatic interaction mediated by Asp59. This interaction helps to recognize the residue Lys145, which is located in the middle of the conserved LXXLL motif. Previous studies found that Lys145 can be recognized by Asn312 in PPARγ LBD (PDB code:3CS8) (Li et al., 2008). Structural comparison between GR and PPARγ in complex with PGC1α shows that PPARγ Asn312 aligns with AncGR2 Asp59 (**Supplemental Figure 6**). This indicates a general mechanism of accommodating a charged residue in the middle of the conserved LXXLL motif by electrostatic interaction. Mutations acting to disrupt this interaction were shown to significantly impair the PGC1α-mediated transactivation (Li et al., 2008). Interestingly, primary charge clamps, in particular the one formed with backbone amide group in Leu143, play a less significant role in PGC1α binding and transactivation in TR and PPARγ signaling (Wu et al., 2003; Wu et al., 2002). These results further highlight the crucial role of a secondary charge clamp in recognizing PGC1α by various NR LBDs.

Acknowledgements

Special thanks to Dr. C. Denise Okafor for her detailed guidance in performing MD simulations and data analysis. The authors want to thank the HDX-MS core in School of Medicine, Emory University for their technical assistance in data collection and analysis. X-ray data were collected at Southeast Regional Collaborative Access Team (SER-CAT) 22-ID beamline at the Advanced Photon Source, Argonne National Laboratory. Supporting institutions may be found at www.ser-cat.org/members/html. Use of the Advanced Photon source was supported by the U.S. Department of Energy, Office of Science, Office of Basic Energy Sciences, under Contract No. W-31-109-Eng-38.

Authorship Contributions

Participated in research design: Liu, Ortlund.

Conducted experiments: Liu, Wang.

Data Analysis: Liu, Wang, Ortlund.

Manuscript writing: Liu, Ortlund.

Accession numbers

The atomic coordinates and structure factors have been deposited in the Protein Data Bank with the accession numbers 6NWK and 6NWL for AncGR2 LBD DEX-PGC1α complex and for AncGR2 LBD HCY-PGC1α complex, respectively.

References

Adams PD, Afonine PV, Bunkoczi G, Chen VB, Davis IW, Echols N, Headd JJ, Hung LW, Kapral GJ, Grosse-Kunstleve RW, McCoy AJ, Moriarty NW, Oeffner R, Read RJ, Richardson DC, Richardson JS, Terwilliger TC and Zwart PH (2010) PHENIX: a comprehensive Python-based system for macromolecular structure solution. *Acta Crystallogr D Biol Crystallogr* **66**(Pt 2): 213-221.

Bledsoe RK, Montana VG, Stanley TB, Delves CJ, Apolito CJ, McKee DD, Consler TG, Parks DJ, Stewart EL, Willson TM, Lambert MH, Moore JT, Pearce KH and Xu HE (2002) Crystal structure of the glucocorticoid receptor ligand binding domain reveals a novel mode of receptor dimerization and coactivator recognition. *Cell* **110**(1): 93-105.

Bostrom P, Wu J, Jedrychowski MP, Korde A, Ye L, Lo JC, Rasbach KA, Bostrom EA, Choi JH, Long JZ, Kajimura S, Zingaretti MC, Vind BF, Tu H, Cinti S, Hojlund K, Gygi SP and Spiegelman BM (2012) A PGC1-alpha-dependent myokine that drives brown-fat-like development of white fat and thermogenesis. *Nature* **481**(7382): 463-468.

Bowerman S and Wereszczynski J (2016) Detecting Allosteric Networks Using Molecular Dynamics Simulation. *Method Enzymol* **578**: 429-447.

Bridgham JT, Ortlund EA and Thornton JW (2009) An epistatic ratchet constrains the direction of glucocorticoid receptor evolution. *Nature* **461**(7263): 515-519.

Chrousos GP (2009) Stress and disorders of the stress system. *Nat Rev Endocrinol* **5**(7): 374-381.

D.A. Case IYB-S, S.R. Brozell, D.S. Cerutti, T.E. Cheatham, III, V.W.D. Cruzeiro, T.A. Darden, R.E. Duke, D. Ghoreishi, M.K. Gilson, H. Gohlke, A.W. Goetz, D. Greene, R Harris, N. Homeyer, S. Izadi, A. Kovalenko, T. Kurtzman, T.S. Lee, S. LeGrand, P. Li, C. Lin, J. Liu, T. Luchko, R. Luo, D.J. Mermelstein, K.M. Merz, Y. Miao, G. Monard, C. Nguyen, H. Nguyen, I. Omelyan, A. Onufriev, F. Pan, R. Qi, D.R. Roe, A. Roitberg, C. Sagui, S. Schott-Verdugo, J. Shen, C.L. Simmerling, J. Smith, R. Salomon-Ferrer, J. Swails, R.C. Walker, J. Wang, H. Wei, R.M. Wolf, X. Wu, L. Xiao, D.M. York and P.A. Kollman (2018) AMBER 2018. *University of California, San Francisco*.

Deng W, Wang Y, Druzak SA, Healey JF, Syed AK, Lollar P and Li R (2017) A discontinuous autoinhibitory module masks the A1 domain of von Willebrand factor. *J Thromb Haemost* **15**(9): 1867-1877.

Emsley P and Cowtan K (2004) Coot: model-building tools for molecular graphics. *Acta Crystallogr D Biol Crystallogr* **60**(Pt 12 Pt 1): 2126-2132.

Floyd RW (1962) Algorithm-97 - Shortest Path. *Commun Acm* **5**(6): 345-345.

Glykos NM (2006) Software news and updates. Carma: a molecular dynamics analysis program. *J Comput Chem* **27**(14): 1765-1768.

Handschin C and Spiegelman BM (2006) Peroxisome proliferator-activated receptor gamma coactivator 1 coactivators, energy homeostasis, and metabolism. *Endocr Rev* **27**(7): 728-735.

He Y, Yi W, Suino-Powell K, Zhou XE, Tolbert WD, Tang X, Yang J, Yang H, Shi J, Hou L, Jiang H, Melcher K and Xu HE (2014) Structures and mechanism for the design of highly potent glucocorticoids. *Cell Res* **24**(6): 713-726.

Henzler-Wildman K and Kern D (2007) Dynamic personalities of proteins. *Nature* **450**(7172): 964-972.

Hollenberg SM and Evans RM (1988) Multiple and cooperative trans-activation domains of the human glucocorticoid receptor. *Cell* **55**(5): 899-906.

Hollenberg SM, Weinberger C, Ong ES, Cerelli G, Oro A, Lebo R, Thompson EB, Rosenfeld MG and Evans RM (1985) Primary structure and expression of a functional human glucocorticoid receptor cDNA. *Nature* **318**(6047): 635-641.

Hughes TS, Chalmers MJ, Novick S, Kuruvilla DS, Chang MR, Kamenecka TM, Rance M, Johnson BA, Burris TP, Griffin PR and Kojetin DJ (2012) Ligand and receptor dynamics contribute to the mechanism of graded PPARgamma agonism. *Structure* **20**(1): 139-150.

Humphrey W, Dalke A and Schulten K (1996) VMD: visual molecular dynamics. *J Mol Graph* **14**(1): 33-38, 27-38.

Kadmiel M and Cidlowski JA (2013) Glucocorticoid receptor signaling in health and disease. *Trends Pharmacol Sci* **34**(9): 518-530.

Kauppi B, Jakob C, Farnegardh M, Yang J, Ahola H, Alarcon M, Calles K, Engstrom O, Harlan J, Muchmore S, Ramqvist AK, Thorell S, Ohman L, Greer J, Gustafsson JA, Carlstedt-Duke J and Carlquist M (2003) The three-dimensional structures of antagonistic and agonistic forms of the glucocorticoid receptor ligand-binding domain: RU-486 induces a transconformation that leads to active antagonism. *J Biol Chem* **278**(25): 22748-22754.

Kendall EC (1951) The development of cortisone as a therapeutic agent. *Antibiot Chemother (Northfield)* **1**(1): 7-15.

Knutti D, Kaul A and Kralli A (2000) A tissue-specific coactivator of steroid receptors, identified in a functional genetic screen. *Mol Cell Biol* **20**(7): 2411-2422.

Knutti D and Kralli A (2001) PGC-1, a versatile coactivator. *Trends Endocrinol Metab* **12**(8): 360-365.

Kohn JA, Deshpande K and Ortlund EA (2012) Deciphering modern glucocorticoid cross-pharmacology using ancestral corticosteroid receptors. *J Biol Chem* **287**(20): 16267-16275.

Kojetin DJ and Burris TP (2013) Small molecule modulation of nuclear receptor conformational dynamics: implications for function and drug discovery. *Mol Pharmacol* **83**(1): 1-8.

Li Y, Kovach A, Suino-Powell K, Martynowski D and Xu HE (2008) Structural and biochemical basis for the binding selectivity of peroxisome proliferator-activated receptor gamma to PGC-1alpha. *J Biol Chem* **283**(27): 19132-19139.

Lin J, Handschin C and Spiegelman BM (2005) Metabolic control through the PGC-1 family of transcription coactivators. *Cell Metab* **1**(6): 361-370.

Lin J, Wu H, Tarr PT, Zhang CY, Wu Z, Boss O, Michael LF, Puigserver P, Isotani E, Olson EN, Lowell BB, Bassel-Duby R and Spiegelman BM (2002) Transcriptional co-activator PGC-1 alpha drives the formation of slow-twitch muscle fibres. *Nature* **418**(6899): 797-801.

Liu X, Speckhard DC, Shepherd TR, Sun YJ, Hengel SR, Yu L, Fowler CA, Gakhar L and Fuentes EJ (2016) Distinct Roles for Conformational Dynamics in Protein-Ligand Interactions. *Structure* **24**(12): 2053-2066.

Mays SG, Okafor CD, Tuntland ML, Whitby RJ, Dharmarajan V, Stec J, Griffin PR and Ortlund EA (2017) Structure and Dynamics of the Liver Receptor Homolog 1-PGC1alpha Complex. *Mol Pharmacol* **92**(1): 1-11.

Motlagh HN, Wrabl JO, Li J and Hilser VJ (2014) The ensemble nature of allostery. *Nature* **508**(7496): 331-339.

Nicholls RA, Fischer M, McNicholas S and Murshudov GN (2014) Conformation-independent structural comparison of macromolecules with ProSMART. *Acta Crystallogr D Biol Crystallogr* **70**(Pt 9): 2487-2499.

Otwinowski Z and Minor W (1997) Processing of X-ray diffraction data collected in oscillation mode. *Methods Enzymol* **276**: 307-326.

Puigserver P, Wu Z, Park CW, Graves R, Wright M and Spiegelman BM (1998) A cold-inducible coactivator of nuclear receptors linked to adaptive thermogenesis. *Cell* **92**(6): 829-839.

Ryckaert J-P, Ciccotti G and Berendsen HJ (1977) Numerical integration of the cartesian equations of motion of a system with constraints: molecular dynamics of n-alkanes. *Journal of Computational Physics* **23**(3): 327-341.

Scarpulla RC, Vega RB and Kelly DP (2012) Transcriptional integration of mitochondrial biogenesis. *Trends Endocrinol Metab* **23**(9): 459-466.

Schacke H, Docke WD and Asadullah K (2002) Mechanisms involved in the side effects of glucocorticoids. *Pharmacol Ther* **96**(1): 23-43.

Schacke H, Rehwinkel H and Asadullah K (2005) Dissociated glucocorticoid receptor ligands: compounds with an improved therapeutic index. *Curr Opin Investig Drugs* **6**(5): 503-507.

Schoch GA, D'Arcy B, Stihle M, Burger D, Bar D, Benz J, Thoma R and Ruf A (2010) Molecular switch in the glucocorticoid receptor: active and passive antagonist conformations. *J Mol Biol* **395**(3): 568-577.

Seitz T, Thoma R, Schoch GA, Stihle M, Benz J, D'Arcy B, Wiget A, Ruf A, Hennig M and Sterner R (2010) Enhancing the stability and solubility of the glucocorticoid receptor ligand-binding domain by high-throughput library screening. *J Mol Biol* **403**(4): 562-577.

Shin DJ, Campos JA, Gil G and Osborne TF (2003) PGC-1alpha activates CYP7A1 and bile acid biosynthesis. *J Biol Chem* **278**(50): 50047-50052.

Suino-Powell K, Xu Y, Zhang C, Tao YG, Tolbert WD, Simons SS, Jr. and Xu HE (2008) Doubling the size of the glucocorticoid receptor ligand binding pocket by deacylcortivazol. *Mol Cell Biol* **28**(6): 1915-1923.

Tokuriki N and Tawfik DS (2009) Protein dynamism and evolvability. *Science* **324**(5924): 203-207.

Wallace AC, Laskowski RA and Thornton JM (1995) LIGPLOT: a program to generate schematic diagrams of protein-ligand interactions. *Protein Eng* **8**(2): 127-134.

Weikum ER, Knuesel MT, Ortlund EA and Yamamoto KR (2017a) Glucocorticoid receptor control of transcription: precision and plasticity via allostery. *Nat Rev Mol Cell Biol* **18**(3): 159-174.

Weikum ER, Okafor CD, D'Agostino EH, Colucci JK and Ortlund EA (2017b) Structural Analysis of the Glucocorticoid Receptor Ligand-Binding Domain in Complex with Triamcinolone Acetonide and a Fragment of the Atypical Coregulator, Small Heterodimer Partner. *Mol Pharmacol* **92**(1): 12-21.

Wu Y, Chin WW, Wang Y and Burris TP (2003) Ligand and coactivator identity determines the requirement of the charge clamp for coactivation of the peroxisome proliferator-activated receptor gamma. *J Biol Chem* **278**(10): 8637-8644.

Wu Y, Delerive P, Chin WW and Burris TP (2002) Requirement of helix 1 and the AF-2 domain of the thyroid hormone receptor for coactivation by PGC-1. *J Biol Chem* **277**(11): 8898-8905.

Yamamoto K, Tamura T, Henmi K, Kuboyama T, Yanagisawa A, Matsubara M, Takahashi Y, Suzuki M, Saito JI, Ueno K and Shuto S (2018) Development of Dihydrodibenzooxepine Peroxisome Proliferator-Activated Receptor (PPAR) Gamma Ligands of a Novel Binding

Mode as Anticancer Agents: Effective Mimicry of Chiral Structures by Olefinic E/ Z-Isomers. *J Med Chem* **61**(22): 10067-10083.

Yoon JC, Puigserver P, Chen G, Donovan J, Wu Z, Rhee J, Adelmant G, Stafford J, Kahn CR, Granner DK, Newgard CB and Spiegelman BM (2001) Control of hepatic gluconeogenesis through the transcriptional coactivator PGC-1. *Nature* **413**(6852): 131-138.

Zhang Y, Castellani LW, Sinal CJ, Gonzalez FJ and Edwards PA (2004) Peroxisome proliferator-activated receptor-gamma coactivator 1alpha (PGC-1alpha) regulates triglyceride metabolism by activation of the nuclear receptor FXR. *Genes Dev* **18**(2): 157-169.

Zoorob RJ and Cender D (1998) A different look at corticosteroids. *Am Fam Physician* **58**(2): 443-450.

Footnotes

This work was supported by National Institutes of Health [R01DK115213] and W. M. Keck Foundation Medical Research Grant to E.A.O. X.L was supported by an American Heart Association postdoctoral fellowship [17POST33660110].

Molecular Pharmacology Fast Forward. Published on August 7, 2019 as DOI: 10.1124/mol.119.116806
This article has not been copyedited and formatted. The final version may differ from this version.

Legends for Figures

Figure 1. DEX binds more tightly to AncGR2 LBD and has higher potency in transactivating GREs than HCY. (A-B) Chemical structures of GR endogenous ligand cortisol/HCY (A) and synthetic ligand DEX (B). Structures show canonical steroid carbon and oxygen atom (in grey circle) numbering. (C) DEX binds to AncGR2 LBD with a tighter K_i than HCY as measured by fluorescence polarization competition with FAM-DEX. (D) DEX transactivates positive GREs with higher potency than HCY. Error bars in both (C) and (D) indicate standard deviation (S.D.) from three replicates and from three independent experiments.

Figure 2. Crystal structures of AncGR2 LBD with PGC1α in complex with DEX and HCY. (A) Overall structure of AncGR2 LBD with DEX (green) bound to PGC1α (purple), with α-helices shown in light blue, β-strands in yellow, and loops in gray. (B and C) 2Fo-Fc omit electron density map (contoured to 2.0 σ) surrounding DEX (B) and HCY (C) in the LBP. (D and E). Extensive hydrogen bonds (dark blue residues) and hydrophobic interactions (light blue residues) are formed between AncGR2 LBD with DEX (D) and HCY(E).

Figure 3. Coregulator binding profiles for AncGR2 LBD in complex with ligands. (A & C) AncGR2 LBD with DEX (A) and HCY (C) was titrated into various FAM-labelled coregulator peptides to monitor fluorescence polarization signal changes to determine binding affinities. These data are represented as mean ± (S.D.) from three replicates and from three independent experiments (B & D). Binding affinities for various coregulator peptides bound to AncGR2 LBD with DEX (B) and HCY (D) are expressed as K_d with 95% confidence interval.

Figure 4. Thermostability of AncGR2 LBD bound to DEX and HCY and in complex with different coregulators. (A & C) Thermal unfolding curves of AncGR2 LBD bound to DEX (A) and HCY (C) in presence of coactivators. (B & D). Thermostability for various coregulators

bound to AncGR2 LBD with DEX (B) and HCY (D) are expressed as Tm ± SD from three replicates and from three independent DSF experiments.

Figure 5. Recognition of PGC1α at the AncGR2 LBD AF-2 surface. (A & B) PGC1α (A) and Tif2 (B) bind to the AncGR2 LBD AF-2 and form extensive hydrophobic contacts, with participating residues in LBD colored in yellow. AncGR2 LBD-DEX-PGC1α structure was used for (A) AncGR2 LBD-DEX-Tif2 (PDB code: 3GN8) was used for (B). (C) Primary charge clamps mediated by Glu224 and Lys48 (shown in blue) hold PGC1α in place. (D). Different primary and secondary charge clamps are formed to mediate the PGC1α (purple) and Tif2 (cyan) binding to AncGR2 LBD.

Figure 6. Differential HDX-MS of AncGR2 LBD-DEX bound to Tif2 and PGC1α. (A). Heat maps of deuterium uptake for AncGR2 LBD-DEX bound to Tif2 and PGC1α. Different time points of LBD incubation in D_2O before measuring deuterium uptake are indicated on the left. (B) Three representative HDX plots of peptic fragments from Tif2- and PGC1α-bound AncGR2 LBD. (C). Differential HDX are mapped on the structure of AncGR2 LBD in complex with DEX. Residues are colored in a continuous gradient from blue to red, with their intensity scaling to the difference in percentage of deuterium exchange [(PGC1α-bound) - (Tif2-bound)]. Residues not covered by any peptides are shown in black.

Figure 7. Allosteric communication between ligand and AFH. (A and B). Cα root mean square fluctuation (RMSF) plots of simulations of AncGR2 LBD with ligands (A) and AncGR2 LBD DEX in complex with coactivators (B). (C). Suboptimal paths connecting nodes Ser227 and ligand (both shown in blue) with edges (shown in orange) displayed. The other nodes in the protein are shown in gray. (D, E, and F). Average values (D) and histograms (E and F) of top

Molecular Pharmacology Fast Forward. Published on August 7, 2019 as DOI: 10.1124/mol.119.116806
This article has not been copyedited and formatted. The final version may differ from this version.

1000 shortest suboptimal paths in AncGR2 with ligands (E) and AncGR2 LBD DEX in complex with coactivators (F).

Molecular Pharmacology Fast Forward. Published on August 7, 2019 as DOI: 10.1124/mol.119.116806
This article has not been copyedited and formatted. The final version may differ from this version.

Table 1. Data Collection and Refinement Statistics

	GR2 LBD-DEX- PGC1α	GR2 LBD-HCY- PGC1α
Data Collection		
Space Group	C 2 2 2_1	C 2 2 2_1
Unit Cell Dimension		
a, b, c (Å)	a=71.8, b=96.4, c=107.9	a=71.8, b=96.4, c=108.2
α, β, γ (°)	90, 90, 90	90, 90, 90
Resolution (Å)	1.64 (1.70-1.64) *	1.60 (1.65-1.60)
R_{pim}	0.068 (0.445)	0.079 (0.297)
CC ½	(0.876)	(0.701)
I/σ	12.2 (1.6)	13.7 (1.8)
Completeness	98.3 (88.8)	99.4 (97.4)
Redundancy	5.5 (3.2)	13.7 (1.8)
Refinement		
No. Reflections	45052 (4009)	49959 (4833)
R_{work}/ R_{free} (%)	18.3/ 20.7	17.9/ 19.4
No. Atoms		
Protein	2174	2225
Ligand	48	81
Water	78	90
B-factors		
Protein	41.1	36.0
Ligand	46.6	51.6
Water	50.1	40.2
R.M.S. deviations		
Bond lengths (Å)	0.01	0.01
Bond angles (°)	1.13	0.82
Ramachandran plot (%)		
Most favored	96.9	95.7
Outliers	0	0

* Values in the parentheses are for the highest-resolution shell.

Molecular Pharmacology Fast Forward. Published on August 7, 2019 as DOI: 10.1124/mol.119.116806
This article has not been copyedited and formatted. The final version may differ from this version.

Figure 1.

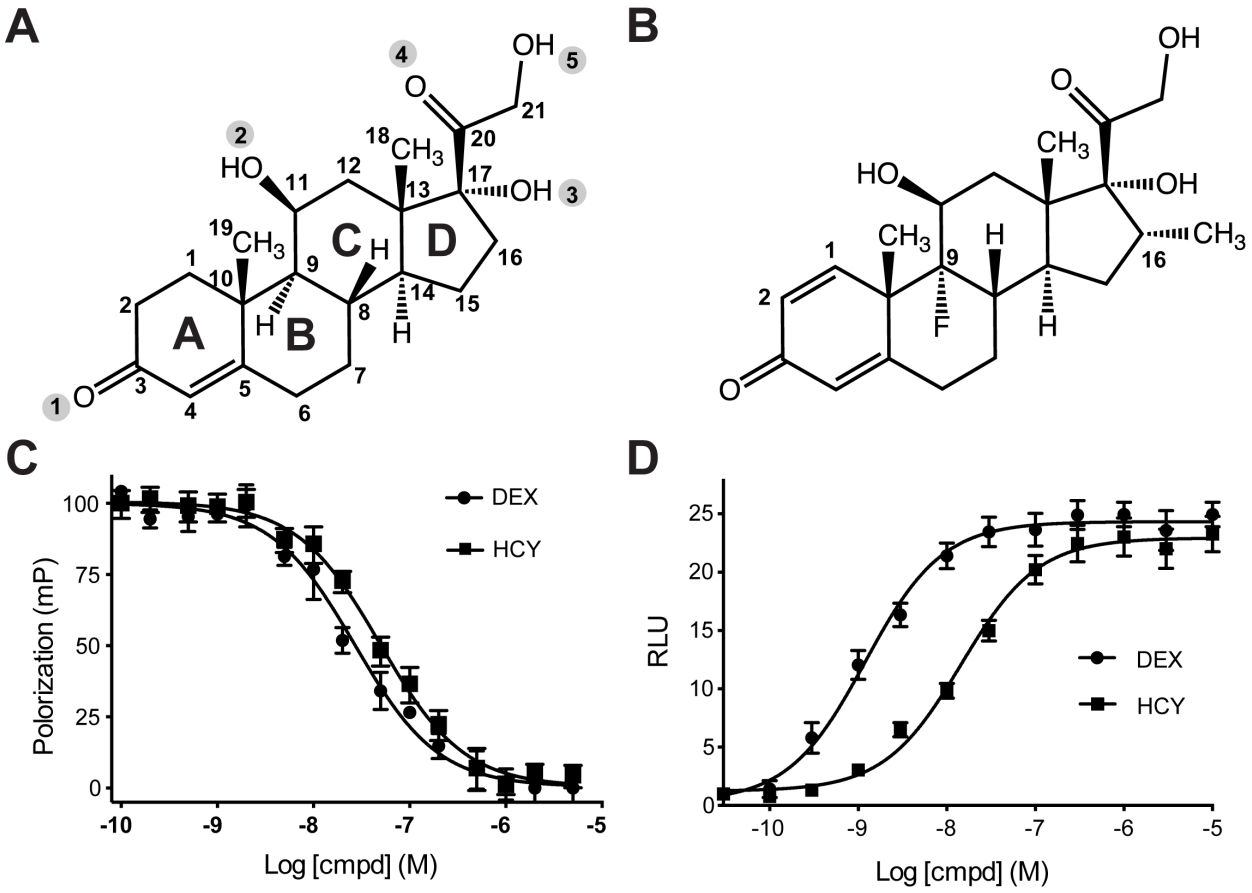

Molecular Pharmacology Fast Forward. Published on August 7, 2019 as DOI: 10.1124/mol.119.116806
This article has not been copyedited and formatted. The final version may differ from this version.

Figure 2.

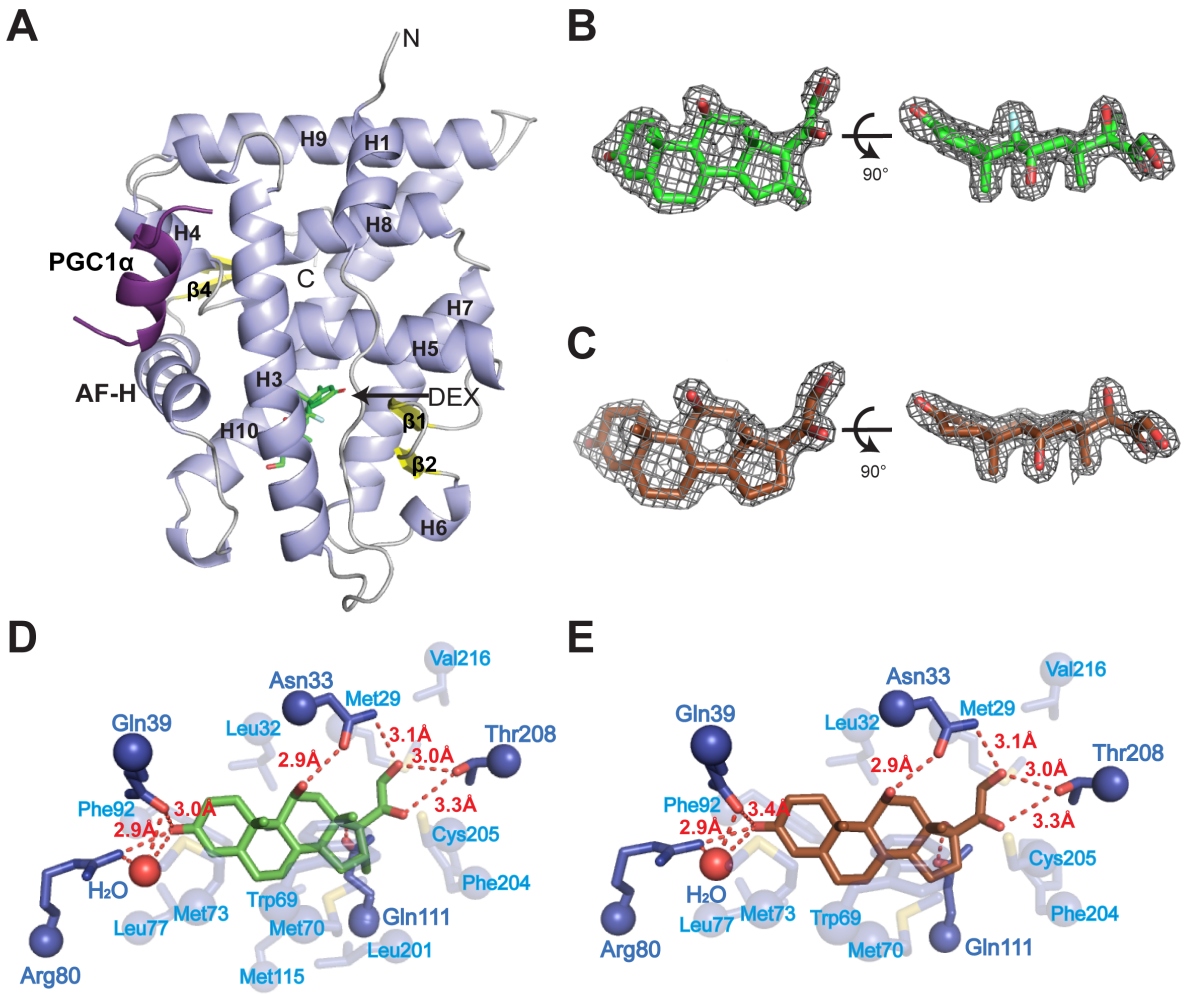

Molecular Pharmacology Fast Forward. Published on August 7, 2019 as DOI: 10.1124/mol.119.116806
This article has not been copyedited and formatted. The final version may differ from this version.

Figure 3.

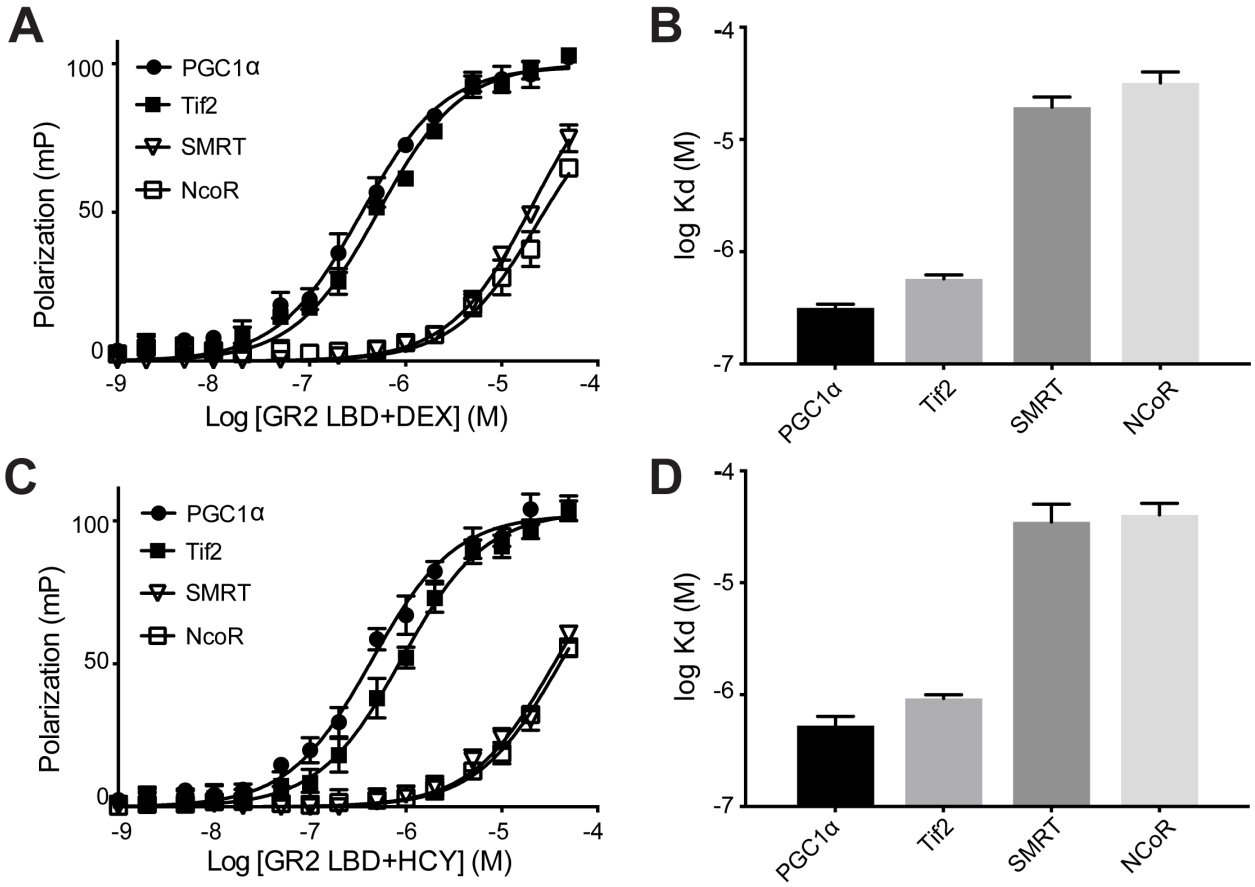

Molecular Pharmacology Fast Forward. Published on August 7, 2019 as DOI: 10.1124/mol.119.116806
This article has not been copyedited and formatted. The final version may differ from this version.

Figure 4.

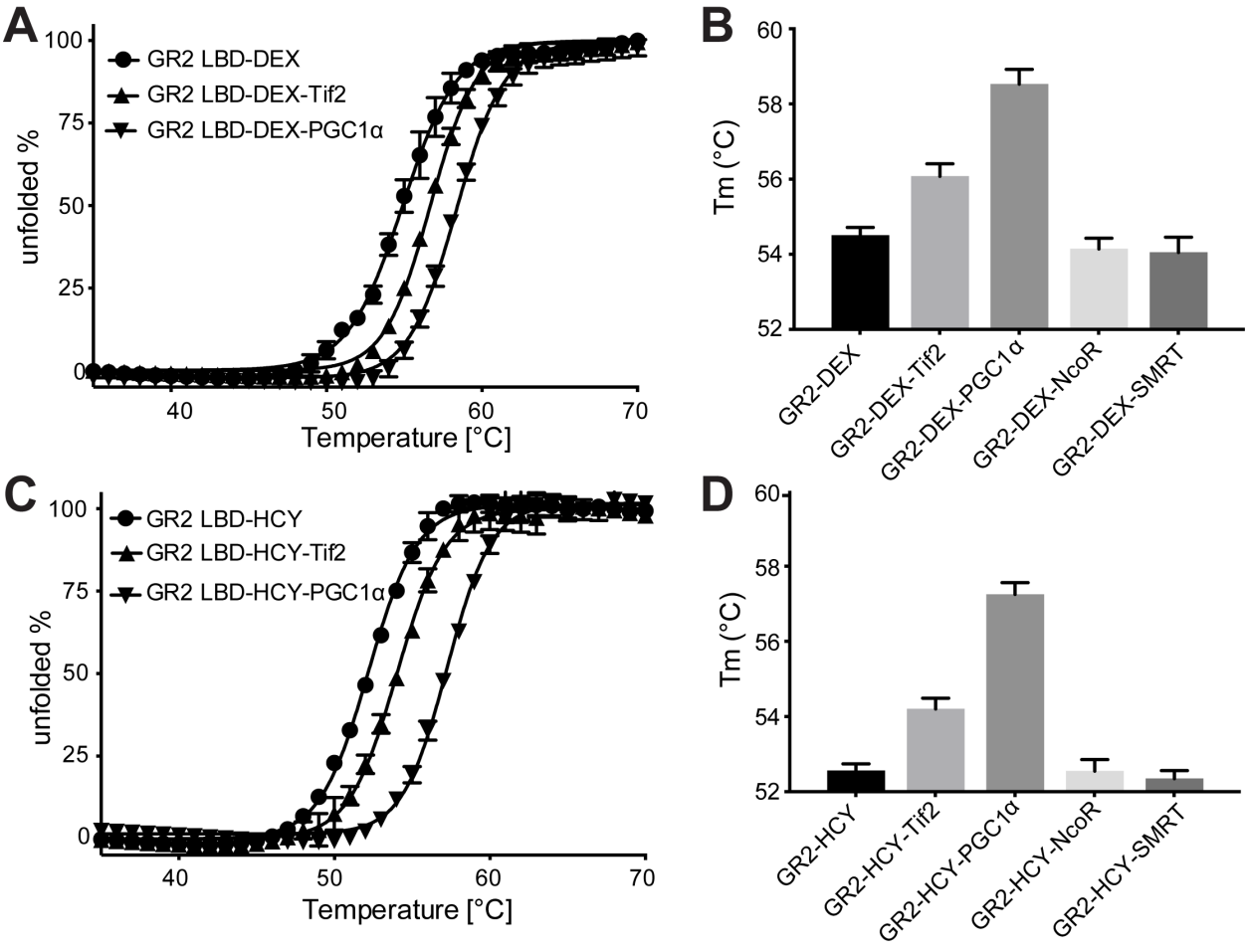

Molecular Pharmacology Fast Forward. Published on August 7, 2019 as DOI: 10.1124/mol.119.116806
This article has not been copyedited and formatted. The final version may differ from this version.

Figure 5.

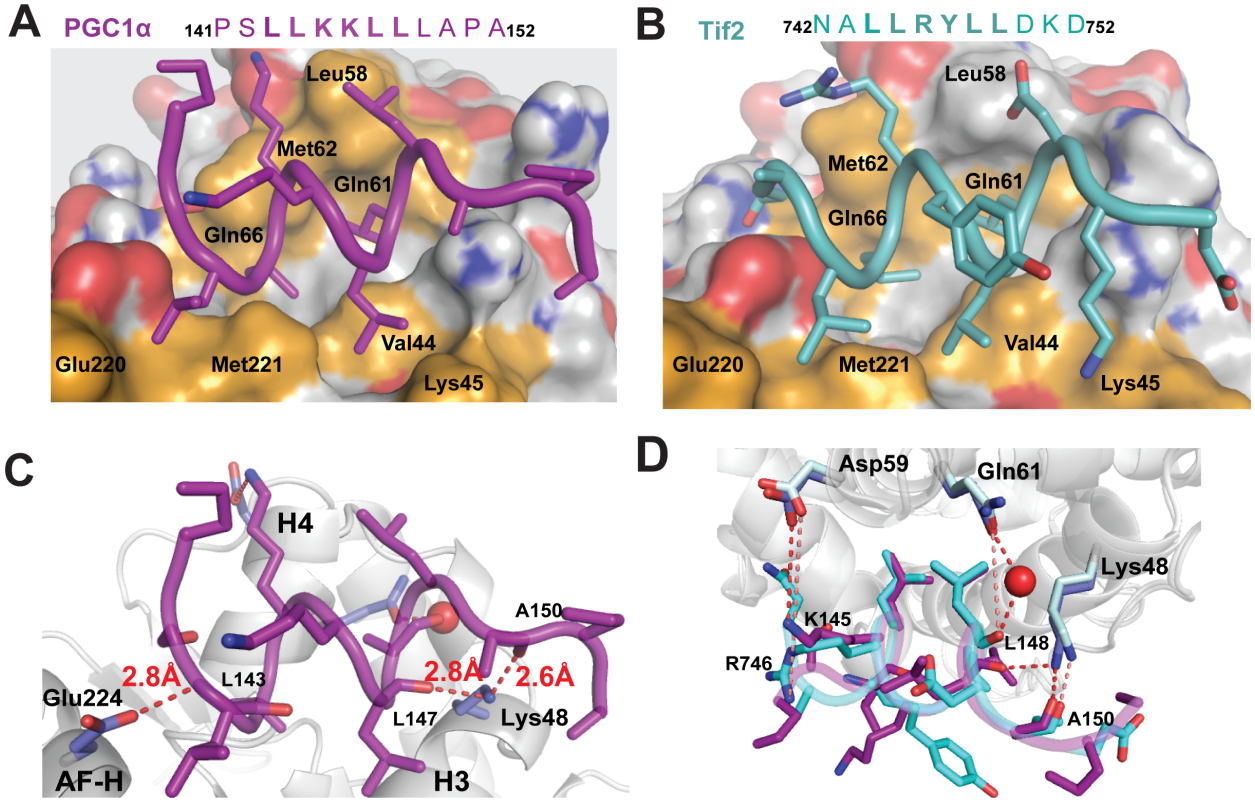

Molecular Pharmacology Fast Forward. Published on August 7, 2019 as DOI: 10.1124/mol.119.116806
This article has not been copyedited and formatted. The final version may differ from this version.

Figure 6.

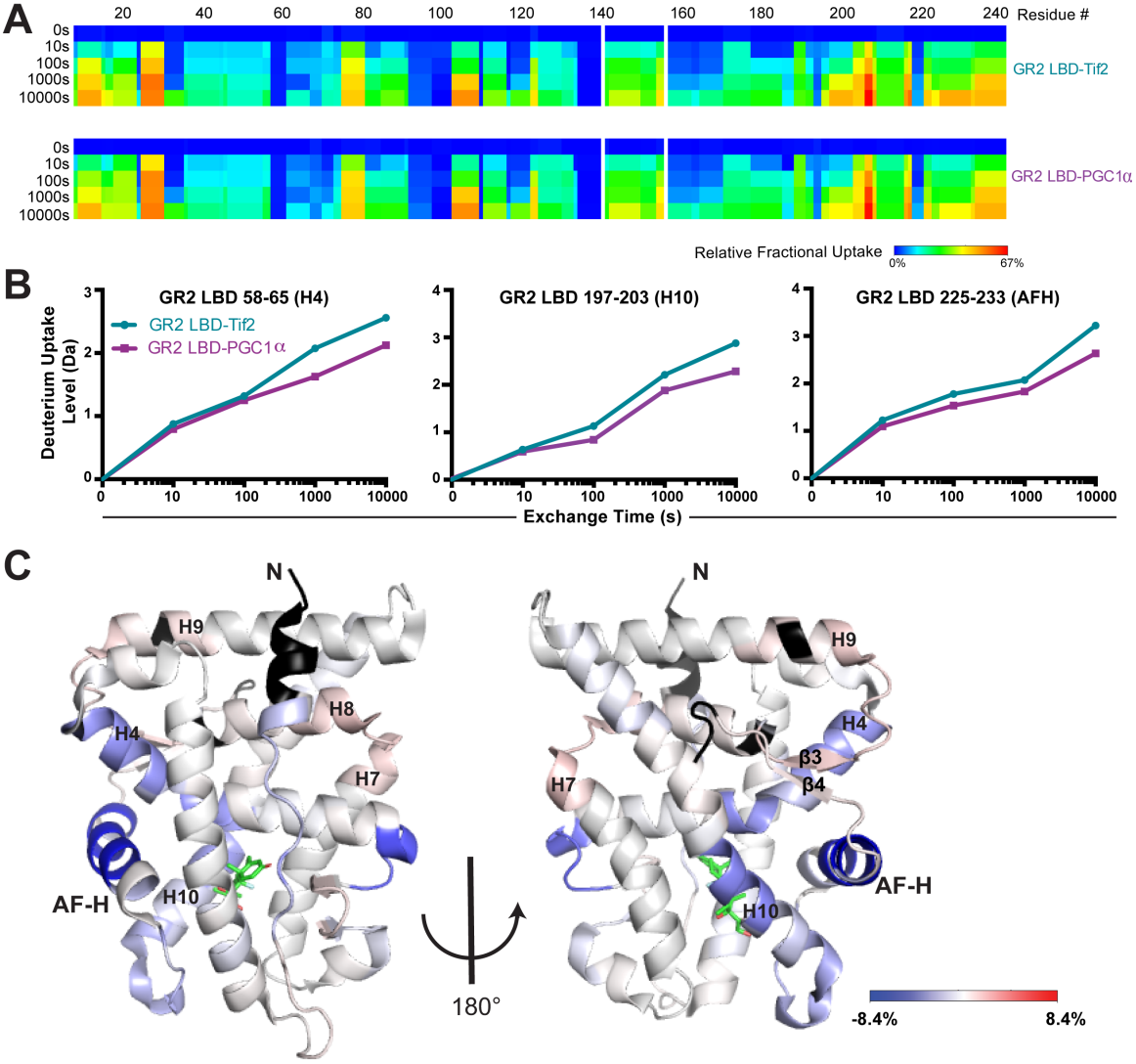

Molecular Pharmacology Fast Forward. Published on August 7, 2019 as DOI: 10.1124/mol.119.116806
This article has not been copyedited and formatted. The final version may differ from this version.

Figure 7.